A Hybrid FEA and MOGA-Based Optimization Framework for Industrial Switched Reluctance Motors

C.E. Abunike[1*], O.I. Okoro[1], C.C. Awah[1], J.U Jeff-Matthew[1], B.I. Oruh[2], A.J. Onah[1]

[1]Dept. of Elect/Elect Engineering, Michael Okpara University of Agriculture, Umudike, Nigeria.
[2]Dept. of Mathematics, Michael Okpara Uni. of Agriculture, Umudike, Nigeria.

ABSTRACT: Switched Reluctance Motors (SRMs) are increasingly used in industrial drives and electric vehicles due to their robust construction, fault tolerance, and wide speed range. However, the non-linear magnetic characteristics of SRMs often lead to torque ripple, vibration, and acoustic noise, posing challenges to achieving optimal performance. This paper presents a Hybrid Finite Element Analysis (FEA) and Multi-Objective Genetic Algorithm (MOGA)-based optimization framework for the industrial design of SRMs. The proposed method integrates accurate electromagnetic simulation using FEA with the Non-Dominated Sorting Genetic Algorithm II (NSGA-II) to optimize key geometric parameters, stator pole arc ratio (*Es*), rotor pole arc ratio (*Er*), and stator yoke height (*Ys*), under multiple objectives and design constraints. The objectives are to maximize average torque and efficiency while minimizing torque ripple and total power loss. Constraints on torque, current density, and temperature are incorporated to ensure thermal and electromagnetic feasibility. Compared with conventional single-objective and unconstrained multi-objective SRM designs, the proposed framework offers a clearly interpretable and reproducible optimization route. It achieves a 71.5 % increase in average torque and reduces torque ripple to 3.18% while satisfying electromagnetic and thermal constraints. The framework's novelty lies in integrating a robust FEA-based evaluation loop with constrained multi-objective decision-making, enabling industrial designers to identify balanced, high-performance SRM geometries efficiently. Future work includes experimental prototyping and machine learning integration to further enhance optimization efficiency.

KEYWORDS: Efficiency, Finite Element Analysis (FEA), Industrial Applications, Multi-objective Genetic Algorithm (MOGA), Switched Reluctance Motor (SRM), Torque Ripple

[Received Mar. 26, 2025; Revised Apr 04, 2025; Accepted Dec 05, 2025] Print ISSN: 0189-9546 | Online ISSN: 2437-2110

I. INTRODUCTION

The relentless pursuit of energy efficiency, reliability, and cost-effectiveness in industrial applications has driven significant advancements in electric motor technologies. Among these, Switched Reluctance Motors (SRMs) have emerged as a promising candidate due to their inherent simplicity, robustness, and ability to operate under harsh conditions (Li *et al.*, 2019). Unlike traditional induction motors or permanent magnet synchronous motors, SRMs do not rely on permanent magnets or windings on the rotor, which reduces manufacturing costs and eliminates concerns related to demagnetization (Abdalmagid *et al*., 2022). Their doubly salient structure enables operation over a wide speed range, making them suitable for electric vehicles, aerospace actuators, and industrial automation systems where mechanical durability and efficiency are essential. Despite these advantages, the design and optimization of SRMs present unique challenges, primarily due to their nonlinear magnetic characteristics, torque ripple, and acoustic noise, which can hinder their performance in industrial applications (Watthewaduge *et al*., 2020). These issues also contribute to reduced torque quality, lower efficiency, and increased mechanical stress on the machine components. Consequently, improving SRM performance through systematic, optimization-driven design approaches has become an active research area focused on balancing torque density, efficiency, torque ripple, and thermal reliability while maintaining manufacturability and cost-effectiveness.

The design of SRMs is inherently multidisciplinary, involving electromagnetic, thermal, and mechanical considerations. Traditional design methodologies often rely on empirical approaches or simplified analytical models, which may not capture the complex interactions between these domains (Oloo and Laszlo, 2025). As a result, there is a growing need for a comprehensive optimization framework that can systematically address these challenges while meeting the stringent performance requirements of industrial applications. This has led to the development of hybrid optimization techniques that combine the strengths of numerical simulations and advanced optimization algorithms (Patel, 2025).

Finite Element Analysis (FEA) has become a cornerstone in the analysis and design of electric machines, including

*Corresponding author: abunike.emmanuel@mouau.edu.ng
doi: http://doi.org/10.63746njtd.v22i5.3543

SRMs. FEA provides a high-fidelity representation of the electromagnetic fields, enabling accurate prediction of performance metrics such as torque, flux linkage, and losses (Liang *et al.*, 2019). However, the computational cost associated with FEA can be prohibitive, especially when dealing with large-scale optimization problems involving multiple design variables and constraints (Raj *et al.*, 2022). To mitigate this, researchers have explored various strategies, including surrogate modeling, reduced-order modeling, and parallel computing (Cheng *et al.*, 2024). Nevertheless, the integration of FEA with optimization algorithms remains a critical area of research, as it directly impacts the efficiency and effectiveness of the design process (Feng et al, 2024).

Multi-Objective Genetic Algorithms (MOGAs) have gained widespread acceptance in the optimization of complex engineering systems due to their ability to handle multiple, often conflicting objectives and constraints (Deb *et al.*, 2002; Opadiji and Ajiboye, 2011). Unlike traditional gradient-based optimization methods, MOGAs do not require derivative information and are well-suited for exploring non-convex and discontinuous design spaces. This makes them particularly attractive for the optimization of SRMs, where the relationship between design variables and performance metrics is often nonlinear and non-intuitive (El-Nemr *et al.*, 2021). By adopting the global search capabilities of MOGAs, designers can identify Pareto-optimal solutions that represent the best trade-offs between competing objectives, such as maximizing torque density while minimizing torque ripple and losses (Abdollahi *et al*., 2022; Abunike *et al*., 2022).

The integration of FEA and MOGA into a unified optimization framework offers a powerful approach to address the challenges associated with SRM design. Such a framework enables the simultaneous consideration of multiple performance metrics, while accounting for the complex interactions between electromagnetic, thermal, and mechanical domains (Patel, 2025). Moreover, it provides a systematic and automated approach to explore the design space, reducing the reliance on trial-and-error methods and accelerating the design process (Ge *et al.*, 2024). However, the development of such a framework requires careful consideration of several key aspects, including the selection of design variables, the formulation of objective functions and constraints, the management of computational resources, and the validation of optimization results (Lei *et al*, 2022).

Recent developments in SRM research have explored various design, control, and optimization approaches to enhance torque density, efficiency, and noise performance. Studies such as those by Ali *et al.*, (2024), Dey *et al.*, (2024), and Patel, (2025) have improved SRM performance through analytical modeling and electromagnetic geometry tuning, while others have applied heuristic optimization algorithms including Genetic Algorithms, Differential Evolution, and Particle Swarm Optimization to identify optimal design parameters. However, many of these works adopt single-objective formulations or neglect the coupling between electromagnetic performance and thermal constraints, which can lead to suboptimal or thermally unstable designs under industrial loading conditions. In addition, several reported frameworks lack a systematic strategy for balancing conflicting objectives such as torque, efficiency, loss, and ripple within a unified design space. Consequently, there remains a research gap in developing a comprehensive, constraint-aware multi-objective optimization framework that combines the accuracy of FEA with the global search capability of evolutionary algorithms. Addressing this gap forms the central motivation of the present study.

Despite the considerable progress in SRM design optimization, most existing approaches either focus on single-objective formulations or overlook the coupled influence of electromagnetic and thermal constraints. Furthermore, few works have systematically linked FEA-based evaluations with a multi-objective optimization framework capable of producing interpretable design trade-offs for industrial use. This study addresses these gaps by proposing a Hybrid FEA plus MOGA-based optimization framework that couples Finite Element Analysis with the Non-Dominated Sorting Genetic Algorithm II (NSGA-II) to achieve high-torque, low-ripple, thermally reliable SRM geometries. The main novelties of this work are:

(i) a constraint-aware, hybridized optimization loop combining accurate FEA models with multi-objective search;

(ii) the use of physically interpretable geometric design variables (stator pole arc ratio *Es*, rotor pole arc ratio *Er*, and stator yoke height *Ys*); and

(iii) a practical decision framework for selecting optimal Pareto-front designs based on industrial torque-first priority.

This methodological integration ensures improved torque density, reduced torque ripple, and better design reproducibility compared with earlier SRM studies.

The motivation for this work stems from the need to develop an optimization framework that can reconcile conflicting design objectives, high average torque, low torque ripple, and minimal power loss, within realistic thermal and electromagnetic limits. Traditional SRM optimization approaches often treat these objectives independently or assume simplified analytical relationships that cannot fully capture nonlinear magnetic saturation and temperature effects. The innovation of this study lies in coupling a high-fidelity finite element model directly with a constrained NSGA-II, thereby creating a robust platform that simultaneously evaluates electromagnetic and thermal responses during optimization. This integration provides a practical pathway toward intelligent, data-driven SRM design suitable for industrial applications where both performance and reliability are critical.

II. SRM TOPOLOGY, MATHEMATICAL MODELING, AND FINITE ELEMENT ANALYSIS (FEA) METHODOLOGY

The SRM considered in this study is a 6/4-pole configuration, consisting of six stator poles and four rotor poles whose parameters are displayed in Table 1. This configuration is widely adopted in industrial applications due to its favorable balance between torque density, efficiency, and ease of manufacturing. The motor operates on the principle of variable reluctance, where torque is generated by the rotor's tendency to align with the energized stator poles in order to minimize the magnetic reluctance along the flux path. Each of the six stator poles is wound with concentrated windings, and windings on diametrically opposite poles are connected in series to form distinct motor phases. The rotor comprises four salient poles and is constructed from laminated steel sheets to effectively reduce eddy current and hysteresis losses. A critical design parameter, the air gap between the stator and rotor, significantly influences the motor's electromagnetic performance, including flux linkage and torque characteristics.

The SRM is powered by an asymmetric half-bridge converter, which sequentially excites the stator phases based on the rotor position. The motor's operation comprises four fundamental stages: alignment, torque production, de-energization, and commutation. Torque is produced due to the variation of inductance with rotor position, and optimal commutation timing is essential to reduce torque ripple and enhance overall efficiency.

To fully understand and predict the electromagnetic and dynamic behavior of the motor, a comprehensive mathematical model is required. The subsequent subsections present the governing equations that define the SRM's operation and performance under various excitation and loading conditions.

The voltage equation for a single phase of the SRM is expressed as follows (Abunike et al, 2021):

$$V = Ri + \frac{d\psi(\theta,i)}{dt}, \tag{1}$$

where V is the applied phase voltage, R is the phase resistance, i is the phase current, $\psi(\theta,i)$ is the flux linkage, which is a function of rotor position (θ) and current (i). The flux linkage $\psi(\theta,i)$ can be expressed as:

$$\psi(\theta,i) = L(\theta,i)i, \tag{2}$$

where $L(\theta,i)$ is the phase inductance, which varies with rotor position and current due to magnetic saturation. The torque produced by a single phase is calculated using the co-energy method:

$$T(\theta,i) = \frac{\partial W'(\theta,i)}{\partial\theta}, \tag{3}$$

where $W'(\theta,i)$ is the co-energy, which can be expressed as follows:

$$W'(\theta,i) = \int_0^i \psi(\theta,i)di, \tag{4}$$

For a linear magnetic circuit (neglecting saturation), the torque can be simplified as follows:

$$T(\theta,i) = \frac{1}{2}i^2\frac{dL(\theta)}{d\theta}. \tag{5}$$

Table 1 Design specifications of the SRM

Parameter	Value
Rated voltage	380 V
Rated speed	1500 rpm
Power output	1.5 kW
Pole numbers	6
Outer diameter	120 mm
Inner diameter	75 mm
Stator pole embrace	0.45
Yoke thickness	12 mm
Frame	Mec100
Pole number	4
Rotor pole embrace	0.3
Yoke thickness	9 mm
Inner diameter	30mm

The mechanical dynamics of the SRM are described by the equation of motion:

$$J\frac{d\omega}{dt} + B\omega = T_e - T_L, \tag{6}$$

where J is the moment of inertia of the rotor, ω is the angular velocity of the rotor, B is the damping coefficient, Te is the electromagnetic torque, Tl is the load torque. The rotor position θ is related to the angular velocity, expressed as follows:

$$\theta = \int \omega dt. \tag{7}$$

The dynamic behavior of the SRM is governed by the interaction between the electromagnetic and mechanical models. The phase currents, rotor position, and angular velocity are coupled as follows using Equations 8 and 9:

$$\frac{di}{dt} = \frac{V - Ri - \frac{\partial\psi(\theta,i)}{\partial\theta}\omega}{L(\theta,i)}, \tag{8}$$

$$\frac{d\omega}{dt} = \frac{T_e - T_L - B\omega}{J}. \tag{9}$$

Furthermore, FEA is employed in this study to accurately model the electromagnetic behavior of the SRM, incorporating nonlinear magnetic properties, saturation effects, and geometric complexities. The FEA simulations are performed using ANSYS Maxwell, a high-fidelity electromagnetic solver capable of addressing both static and transient magnetic field problems.

At the core of the FEA approach are Maxwell's equations, which govern the behavior of electric and magnetic fields. For magnetostatic and low-frequency transient simulations typical of rotating machines, the key equations are (Anees and Angermann, 2019):

$$\nabla\cdot\vec{B} = 0 \text{ (Gauss's Law for Magnetism)}, \tag{10}$$

$$\nabla\times\vec{H} = \vec{J} \text{ (Ampere's Law)}, \tag{11}$$

$$\vec{B} = \mu(\vec{H})\vec{H} \quad \text{(Constitutive Relation)}, \tag{12}$$

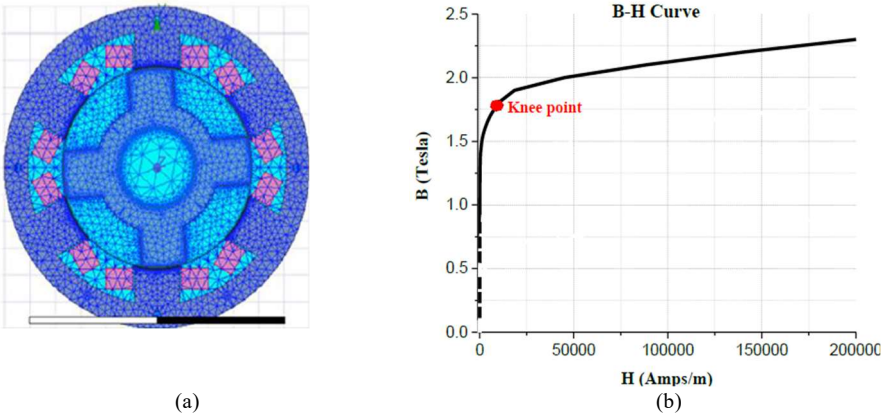

(a) (b)

Figure 1 Properties of the SRM: (a) Mesh map in Maxwell 2D, (b) Magnetic characteristics of the core material

where $\vec{B}$ is the magnetic flux density, $\vec{H}$ is the magnetic field intensity, $\vec{J}$ is the current density, $\mu(\vec{H})$ is the magnetic permeability, which is nonlinear and varies with $\vec{H}$ for ferromagnetic materials. For time-varying fields (quasi-static approximation), Faraday's Law is also included:

$$\nabla \times \vec{E} = -\frac{\partial \vec{B}}{\partial t}, \tag{13}$$

and the electric field $\vec{E}$ and current density $\vec{E}$ are related by:

$$\vec{J} = \sigma \vec{E}, \tag{14}$$

where σ is the electrical conductivity. These equations are solved numerically using the finite element method across the motor's discretized geometry.

A 2D cross-sectional geometry of the 6/4 SRM is discretized into a finite element mesh as shown in Figure 1(a), with refined meshing applied in regions where magnetic flux density is expected to be high, such as the air gap and pole tips, to ensure numerical accuracy. The stator and rotor cores are modeled using the nonlinear B-H characteristics of laminated M19 silicon steel, capturing the effects of magnetic saturation. The material's B-H curve is depicted in Figure 1(b). The windings are modeled as copper conductors with an electrical resistivity of ρ=1.68×10^{-8} Ωm. To reduce computational time and exploit the motor's symmetry, periodic boundary conditions are applied, limiting the simulation domain to a single pole pair. This approach retains solution fidelity while significantly lowering the computational cost. The stator windings are energized using current waveforms corresponding to typical operating conditions. The rotor is set to rotate at a specified mechanical speed, and the motion setup includes the electromechanical interaction between stator and rotor, enabling a realistic assessment of motor performance under load.

III. GENETIC ALGORITHM OPTIMIZATION AND HYBRID FRAMEWORK

This section describes the integrated FEA and MOGA framework developed to optimize the SRM design for industrial performance. The optimization procedure follows the structured workflow illustrated in Figure 2, where electromagnetic and thermal performance metrics are evaluated iteratively to identify Pareto-optimal design solutions.

The optimization process begins with initial sizing of the SRM based on predefined operating requirements such as target torque, speed, and power output. Key geometric parameters are estimated using analytical methods to ensure the baseline design operates within feasible limits. Following this, parametric analysis is conducted by defining a feasible design space bounded by key geometric variables. The three primary design variables considered in this study are: Stator pole arc ratio (E_s), Rotor pole arc ratio (E_r), and Stator yoke height (Y_s).

The design space is bounded as follows:

$$0.25 \leq E_s \geq 0.5, 9\,mm \leq Y_s \geq 13\,mm, 0.25 \leq E_r \geq 0.5 \tag{15}$$

Each combination of these parameters defines a unique SRM geometry, which is then evaluated through FEA. The optimization problem is formulated as a multi-objective minimization and maximization task, seeking to (i) maximize average torque T_{avg},, (ii) maximize efficiency η, (iii) minimize torque ripple T_{rip}, (iv) minimize total losses P_{total} =P_{cu}+P_{core}, and (v) maintain peak flux density B_m and thermal constraints Temp (wind.) ≤ 150^0C, Temp (lam.) ≤ 100^0C.

Mathematically, the multi-objective formulation can be expressed as follows:

$$\max f_1(x) = T_{avg}(x) \tag{16}$$

$$\max f_2(x) = \eta(x) \tag{17}$$

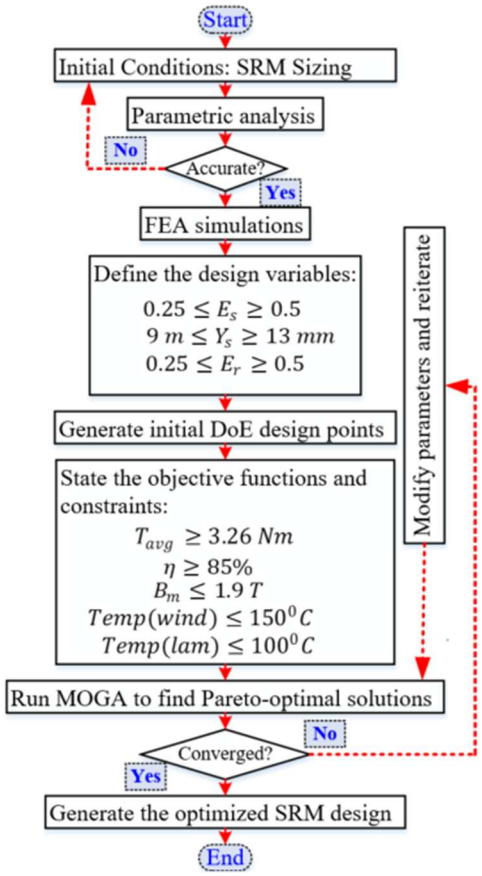

Figure 2 Hybrid FEA–MOGA optimization framework for SRM design, where the MOGA directly interfaces with the FEA solver for each evaluation.

$$\min f_3(x) = T_{rip}(x) \tag{18}$$

$$\min f_4(x) = P_{total}(x) \tag{19}$$

subject to:

$$T_{avg} \geq 3.26\ Nm \tag{20}$$

$$\eta \geq 85\% \tag{21}$$

$$B_m \leq 1.9\ T \tag{22}$$

$$Temp(wind.) \leq 150^0C \tag{23}$$

$$Temp(lam.) \leq 100^0C \tag{24}$$

$$x = \{E_s, Y_s, E_r\}. \tag{25}$$

Where x denotes the design variable vector. In the optimization setup, a minimum average torque constraint of 3.26 Nm was imposed to ensure that all candidate designs met the baseline performance requirement observed during the preliminary analytical stage.

A Design of Experiments (DoE) is performed to generate the initial sample points from the design space. Each DoE point represents a unique combination of $\{E_s, E_r, Y_r\}$ as displayed in Table 2 where P1, P2, P3, P4, P5, P6, and P7 represent E_s, Y_s and E_r, T_{avg}, η, T_{rip}, and P_{total}, respectively. For each design point, the FEA simulation evaluates the performance metrics.

Subsequently, a MOGA is employed to search for Pareto-optimal solutions. MOGA evolves the population through selection, crossover and mutation, driven by a fitness function incorporating the objective metrics and penalty functions for any constraint violations. In this study, the Non-dominated Sorting Genetic Algorithm II (NSGA-II) is adopted as the MOGA framework. A population size of 100 individuals and 20 generations were used, resulting in a total of 2,000 evaluated designs. Crossover and mutation probabilities were set to 0.8 and 0.1, respectively, values that provide a balance between exploration and convergence for design spaces of moderate dimensionality. The statement "maximum design candidates per generation = 3" referred only to the three best non-dominated solutions that were extracted from each generation for convergence monitoring and comparison, not to a limitation of the population size. The full NSGA-II

Table 2 Design solutions of DoE

S/N	P1	P2 (mm)	P3	P4 (Nm)	P5 (%)	P6 (%)	P7 (W)
1	0.375	11.650	0.375	3.964	9.107	98.23	37.86
2	0.250	11.650	0.375	4.737	12.025	98.61	35.37
3	0.500	11.650	0.375	2.683	5.562	97.28	39.92
4	0.375	10.500	0.375	3.904	9.007	98.11	39.92
5	0.375	12.800	0.375	4.027	9.236	98.32	36.62
6	0.375	11.650	0.250	3.642	9.215	94.61	110.26
7	0.375	11.650	0.500	2.238	4.505	96.54	42.58
8	0.273	10.715	0.273	3.475	8.054	96.16	73.70
9	0.477	10.715	0.273	3.721	9.621	98.12	37.84
10	0.273	12.585	0.273	3.636	8.334	96.29	74.36
11	0.477	12.585	0.273	3.856	9.826	97.16	59.88
12	0.273	10.715	0.477	3.777	8.034	80.17	496.43
13	0.477	10.715	0.477	1.499	2.747	94.07	50.17
14	0.273	12.585	0.477	3.575	8.208	94.21	116.74
15	0.477	12.585	0.477	1.529	2.822	93.95	52.33

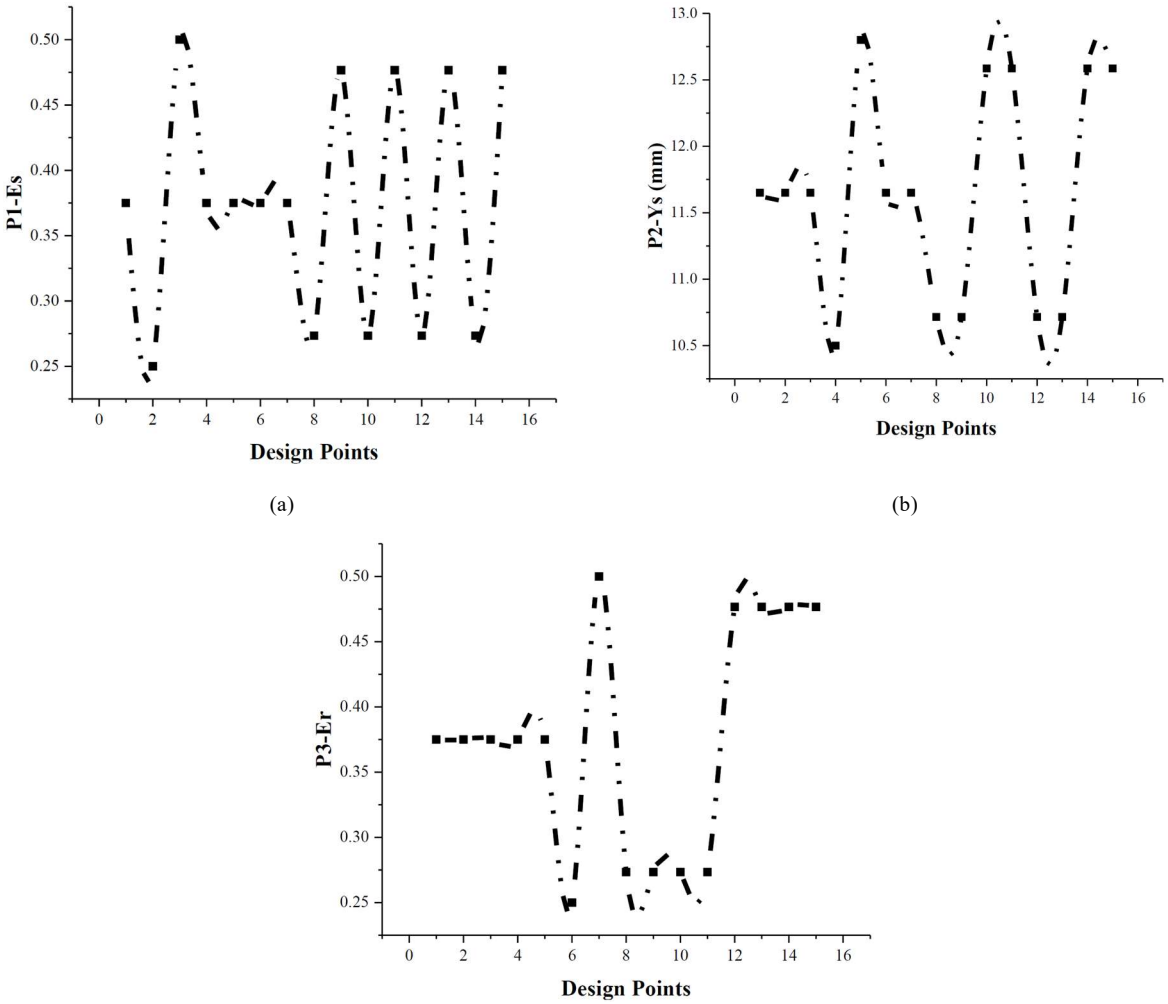

Figure 3 Variation of geometric design parameters: (a) E_s with design points, (b) Y_s with design points, (c) E_r with design points.

population was evaluated at every iteration, ensuring sufficient diversity and convergence reliability. These settings were selected based on preliminary sensitivity runs that confirmed stable Pareto-front formation beyond 100 × 20 evaluations. Among the multiple objectives, average torque is assigned the highest design priority, followed by efficiency, average torque ripple, and total loss in that order. As a result, the final selected design is one that maintains strong average torque integrity, while achieving desirable efficiency and acceptable levels of torque ripple and loss. The optimization loop will then iteratively refines the design variable set. If the convergence criterion (based on Pareto front stability and fitness improvement) is not met, the algorithm modifies the parameters and re-evaluates them through FEA, as shown by the red feedback loop in Figure 2.

IV. RESULTS AND DISCUSSION

This section presents and discusses the results of the optimization process using the hybrid FEA and MOGA framework. The optimization was conducted across 16 design points generated via a DoE, each evaluated based on geometric variation and electromagnetic performance. The primary focus is on the effects of design variables on the motor's key performance indicators: average torque, torque ripple, efficiency, and total losses.

Figure 3 shows the variation of the three selected design variables, E_s, Y_s, E_r, across the 16 evaluated design points. Figure 3(a) reveals that the E_s varies within the defined range of 0.25 to 0.50, with notable fluctuations across design points. These variations influence flux linkage and magnetic saturation in the stator teeth, which in turn affect the torque output and inductance profile. In Figure 3(b), the Y_s shows changes between 10.5 mm and 13 mm. This parameter directly impacts the magnetic path length and the reluctance of the rotor core. Insufficient yoke height can lead to flux crowding and magnetic saturation, while excessive height contributes to increased core losses and rotor inertia. Figure 3(c) illustrates the E_r distribution, ranging between 0.25 and 0.50. This ratio

is critical in shaping the torque profile and minimizing torque ripple. Lower values can produce sharper torque peaks, whereas higher values yield smoother but potentially lower torque outputs. These variations collectively define the electromagnetic geometry of the SRM and are key contributors

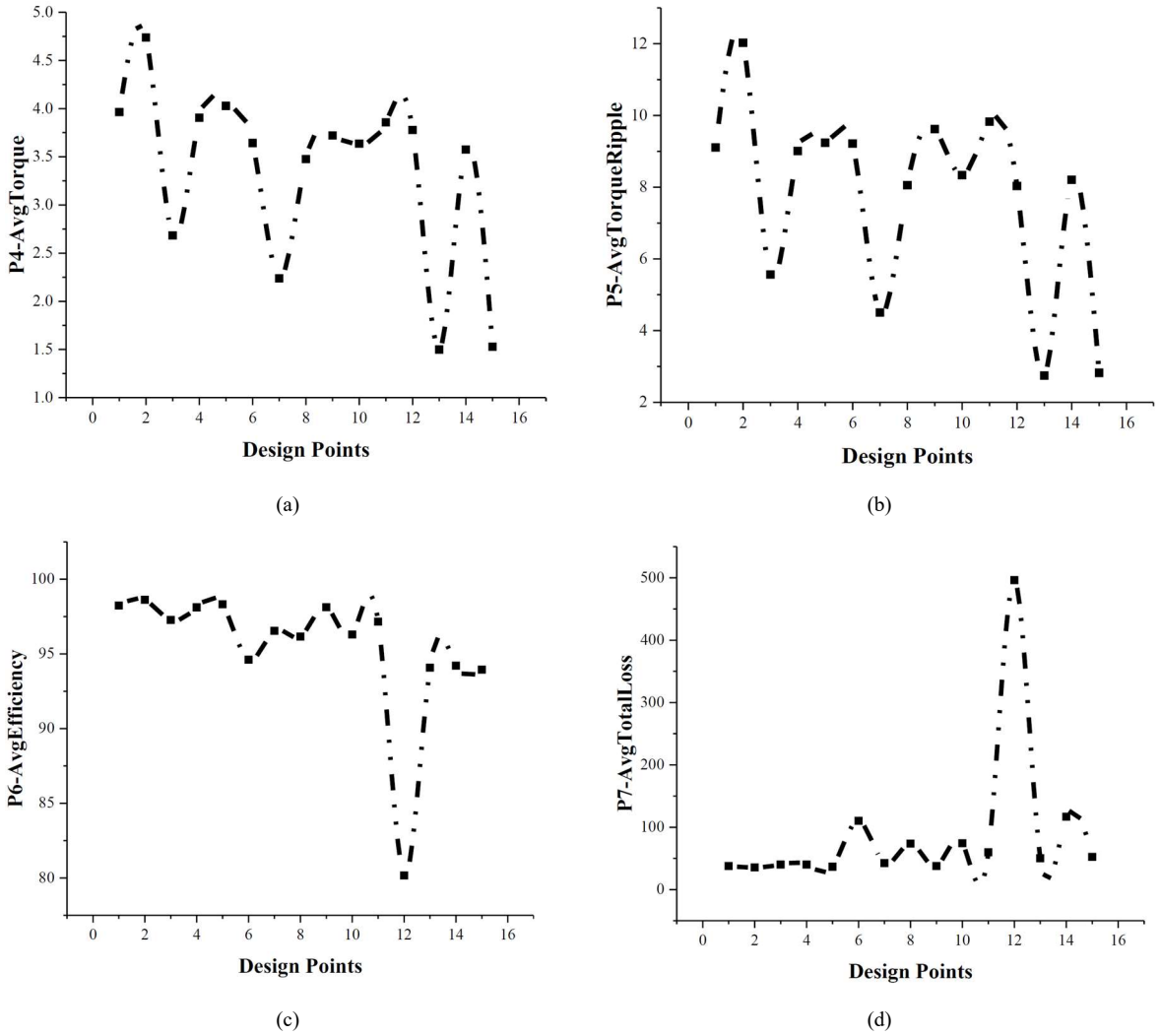

Figure 4 Variation of performance metrics: (a) T_{avg} with design points, (b) T_{rip} with design points, (c) η with design points, (d) P_{total} with design points.

to the performance variations observed in the subsequent plots.

Figure 4 presents the performance evaluation of each SRM configuration in terms of average torque, torque ripple, efficiency, and total losses. As shown in Figure 4(a), the average torque varies significantly across design points, ranging from just over 1.5 Nm to nearly 4.8 Nm. Designs with optimized combinations of E_s, E_r, and Y_s yield higher torque output, particularly those around points 1, 4, and 14. These results confirm that a balanced stator-rotor pole interaction is essential for maximizing torque. Figure 4(b) shows the variation in torque ripple, with values ranging from approximately 3% to over 12%. Designs with high torque ripple often coincide with rapid changes in inductance due to poorly aligned pole arcs or inadequate commutation timing. Lower ripple is observed in design points where the rotor and stator arcs are well synchronized, especially in the mid to high range of E_r. The average efficiency, displayed in Figure 4(c), remains above 90% for most design points but drops significantly around design point 12. This suggests that despite high torque outputs in some configurations, losses due to saturation or thermal limitations may compromise efficiency if not properly balanced. Figure 4(d) illustrates the average total losses (combination of core and copper losses). Most designs maintain loss levels under 100 W, except for one extreme spike observed around design point 12, which correlates with a drop in efficiency. This behavior reflects localized magnetic saturation and increased copper losses due to suboptimal winding-resistance interaction.

To further understand the influence of each design parameter on the SRM's performance, a sensitivity analysis was conducted using the results from the FEA simulations and the DoE. The sensitivity chart presented in Figure 5 quantifies the normalized effect of each design variable on the four output parameters. Several important trends are observed: E_s has a strong negative sensitivity with respect to average torque,

torque ripple, and efficiency. This indicates that increasing E_s generally leads to a reduction in torque output and efficiency, while increasing torque ripple. This can be attributed to magnetic flux saturation and poor alignment between the stator and rotor poles when the stator arc is excessively wide. Conversely, Y_s exhibits positive sensitivity across all output parameters except total losses. An increase in Y_s tends to

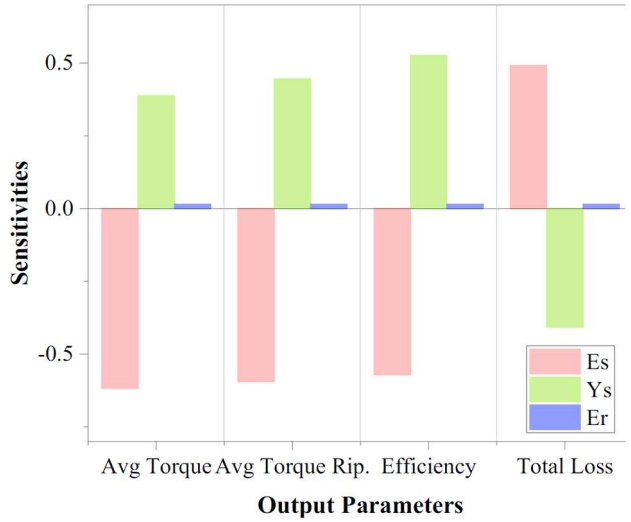

Figure 5 Sensitivity of SRM Design Variables to Performance Metrics.

improve average torque, reduce torque ripple, and enhance efficiency, due to better magnetic flux conduction and reduced saturation in the rotor back iron.

However, a larger yoke height may result in an increase in total loss, possibly due to increased core volume and iron losses. E_r, in contrast, shows minimal sensitivity across all output metrics. This suggests that E_r within the specified design range, does not have a dominant influence on the motor's performance compared to E_s and Y_s. Nonetheless, it may still contribute marginally to the shape of the inductance profile and smoothness of torque output. Overall, the sensitivity analysis provides valuable insights for decision-making during the design phase. Specifically, it suggests that the stator pole arc ratio must be carefully constrained to avoid negative performance impacts, while rotor yoke height can be strategically adjusted to improve torque and efficiency. The rotor pole arc ratio appears to offer less optimization leverage, at least within the current parametric bounds. Although the sensitivity analysis in Figure 5 indicates that an isolated increase in the E_s tends to reduce T_{avg}, this reflects only the local derivative effect when the other variables remain fixed at their baseline levels. During multi-objective optimization, however, E_s interacts strongly with Y_s and E_r. The simultaneous adjustment of these variables can offset the local negative influence of E_s and lead to a global increase in T_{avg}. In the final Pareto-optimal configuration, for instance, a moderate rise in E_s from 0.25 to 0.38, combined with a reduction in Y_s and a slight change in E_r, produced an overall 71.5 % increase in average torque. Hence, the sensitivity trend and the optimization outcome are consistent when multivariate interactions are considered.

To gain deeper insight into the influence of individual design variables on SRM performance, a response surface analysis was conducted. The results are shown in Figure 6, which illustrates how variations in Y_s and E_s affect key performance metrics: average torque, torque ripple, efficiency, and total losses. These analyses enable the identification of optimal regions within the design space and help visualize trade-offs among objectives. The parameter pairs shown in Figure 6 were selected based on the sensitivity analysis results, which identified these variables as having the highest combined influence on average torque and torque ripple. This choice highlights the most dominant interactions rather than exhaustively covering all parameter combinations. Figure 6(a) demonstrates a strong positive correlation between Y_s and T_{avg}. As Y_s increases from 10.5 mm to 13.0 mm, the average torque improves steadily from approximately 5.5 Nm to 5.62 Nm. This behavior is attributed to the increased magnetic path area in the rotor back iron, which reduces flux saturation and enhances torque production. In Figure 6(b), average torque ripple also increases with Y_s, rising from just above 3.05 to about 3.35. Although higher Y_s values improve torque, they also amplify torque ripple, possibly due to the increased magnetic energy variations during rotor rotation. This introduces a performance trade-off that must be carefully managed. Figure 6(c) presents a non-linear relationship between Y_s and efficiency. A peak efficiency of about 96.35% is observed around Y_s = 10.6 mm, while local dips appear near 12.3 mm. This suggests that while higher yoke heights promote torque, they may also increase iron losses, which in turn reduce efficiency. Thus, an optimal Y_s exists that balances torque production and energy efficiency. Figure 6(d) evaluates the effect of E_s on average total loss. The loss curve shows a distinct U-shaped profile, with the minimum losses (~26 W) observed around E_s = 0.3. Beyond this point, total losses increase significantly, peaking at approximately 48 W near E_s = 0.48. A wider stator pole arc increases the magnetic flux path length, resulting in higher core losses due to saturation and hysteresis effects. These response surfaces confirm earlier sensitivity findings—specifically, that Y_s has a critical role in defining the torque-efficiency balance, while E_s primarily governs loss characteristics. As such, multi-objective optimization must consider both to ensure robust performance across varying load conditions.

The final stage of the optimization process involves identifying Pareto-optimal solutions using the NSGA-II framework. The Pareto front represents a set of non-dominated solutions where improvement in one objective would lead to degradation in another, thereby offering optimal trade-offs. Figure 7 illustrates four Pareto front trade-off plots that visualize the relationships between key conflicting objectives. The "candidate point" denotes the best design solution identified from the set of Pareto-optimal options. It is selected based on its strategic location on the front close to the knee

region where significant gains in one metric are no longer possible without considerable sacrifices in others.

Figure 7(a) plots T_{avg} versus η. The upward-sloping Pareto front shows that higher efficiency is generally achievable with an increase in average torque. The "candidate point" identified along this front represents a solution with a well-balanced trade-off, offering both high torque and high efficiency, which aligns with the primary objective priorities of this study. Figure 7(b) shows the relationship between T_{rip} and η. A clear trade-off is visible: designs with minimal ripple tend to operate at slightly lower efficiency. The candidate point chosen balances this trade-off, ensuring acceptable ripple levels while maintaining high efficiency. Figure 7(c) presents the interaction between T_{avg} and P_{total}.

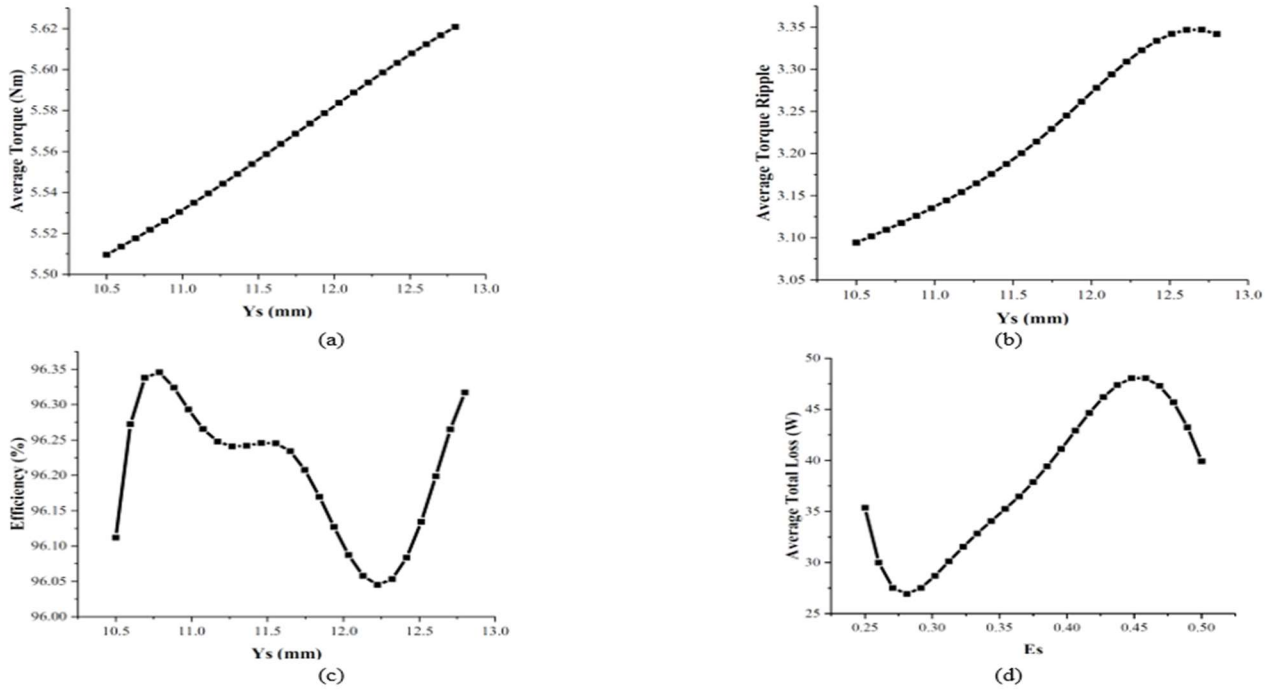

Figure 6 Response Surface Behavior of Output Metrics with Respect to SRM Geometric Parameters: (a) T_{avg} vs. Y_s, (b) T_{rip} vs. Y_s, (c) η vs. Y_s, (d) P_{total} vs. E_s.

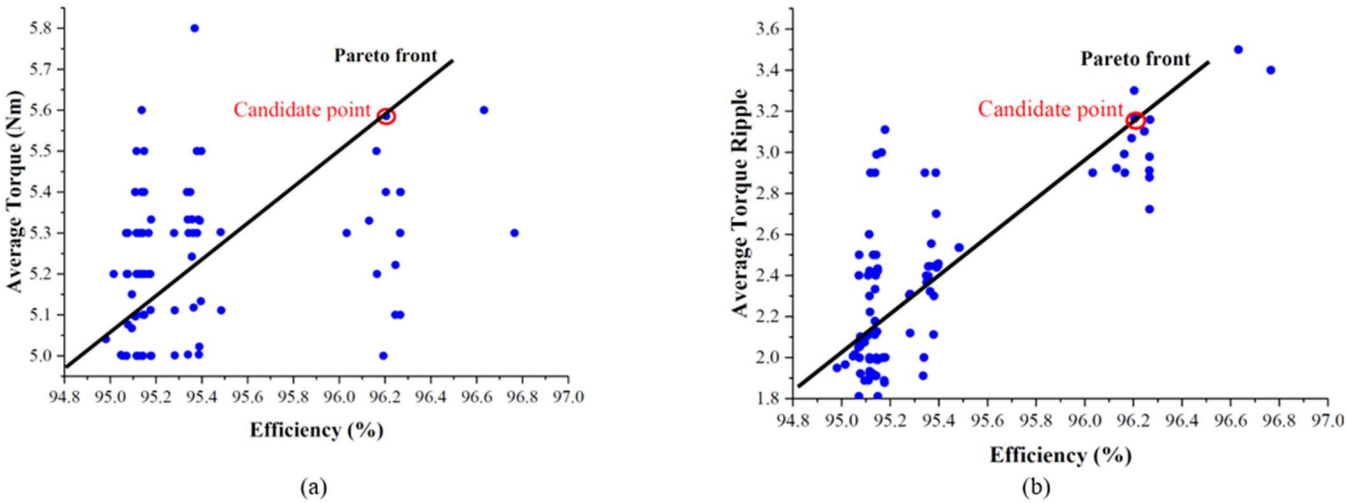

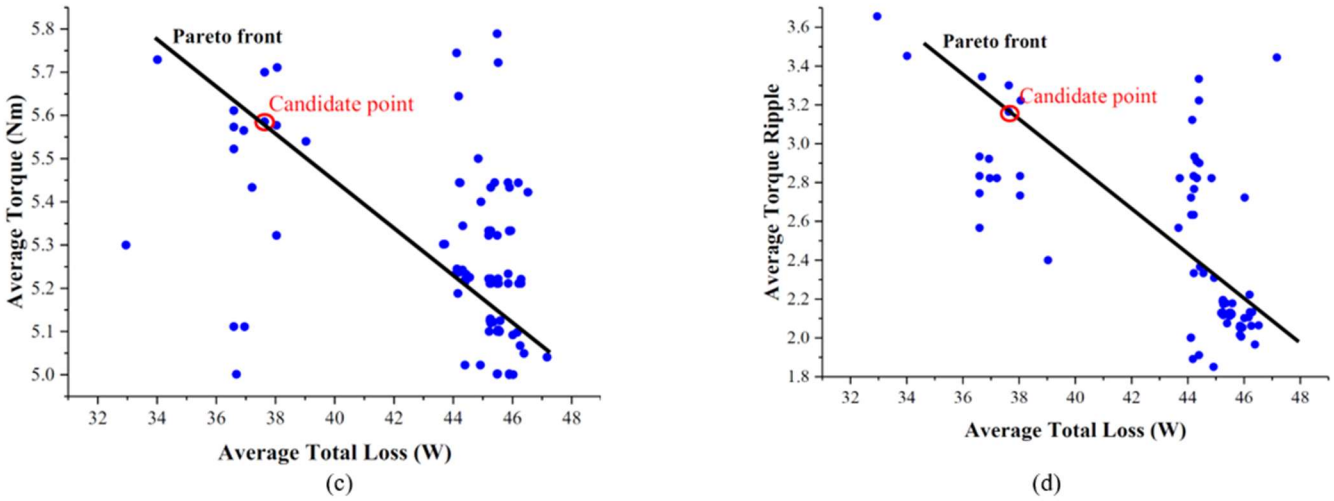

Figure 7 Pareto front analysis of trade-offs between key SRM performance objectives: (a) T_{avg} vs. η, (b) T_{rip} vs. η, (c) T_{avg} vs. P_{total}, (d) T_{rip} vs. P_{total}.

Table 3 Comparison of Initial and Optimized SRM Design Parameters and Performance Metrics, with Percentage Variation

Parameter	Value	Unit	Variation (%)
E_s	0.25	0.38	52.00
E_r	0.25	0.38	52.00
Y_s (mm)	9.00	11.65	29.44
T_{avg} (Nm)	3.26	5.59	71.47
T_{rip} (%)	3.26	3.18	-2.45
η (%)	85.00	96.20	13.18
P_{total} (W)	41.00	37.63	-8.22
Temp (wind.) (^{0}C)	150.00	143.20	-4.53

The inverse relationship indicates that designs achieving higher torque also incur higher losses. The Pareto front confirms that there are no solutions with both maximum torque and minimum losses. The candidate point is selected to maintain torque integrity while controlling the total loss within acceptable limits. Figure 7(d) illustrates a similar inverse trend between T_{rip} and P_{total}. As ripple decreases, total losses increase due to control strategy and magnetic loading effects. The selected design reflects a compromise between minimizing torque ripple and maintaining acceptable losses. These Pareto plots validate the effectiveness of the multi-objective optimization strategy. They demonstrate that the selected candidate design point satisfies the problem's constraints and reflects the objective priorities as displayed in Table 3. Among the Pareto-optimal solutions generated by the NSGA-II algorithm, the final design was selected based on engineering judgment, prioritizing a balanced trade-off between torque enhancement and torque-ripple suppression. The chosen configuration corresponds to the "knee point" of the Pareto front, where further torque gains would result in disproportionately higher ripple or losses. This selection strategy ensures a practical and stable design suitable for industrial SRM applications without relying on arbitrary or single-objective maximization.

The selected candidate design was validated through a refined FEA simulation under nominal operating conditions. The following key observations were made:
(i) T_{avg} exceeded the minimum constraint (3.26 Nm) by a wide margin, achieving 5.59 Nm, indicating a high-power density suitable for industrial applications;
(ii) η remains above 96%, demonstrating good electromagnetic utilization and low core/copper losses, thereby satisfying the imposed efficiency threshold;
(iii) Although the reduction in T_{rip} (–2.45%) appears small, it reflects a controlled trade-off during optimization, where torque enhancement was prioritized while maintaining ripple within acceptable limits (3.18%) to ensure smooth torque output and reduced vibration; and
(iv) Thermal limits for winding and lamination temperatures are not exceeded, ensuring the long-term reliability and insulation safety of the machine.

Moreover, the selected geometry strikes a balance across all objectives, as illustrated by its strategic location on the Pareto front. The low value of stator arc ratio (E_s = 0.38) contributes to minimal core losses, while the moderate rotor yoke height ensures high magnetic efficiency and acceptable thermal behavior. These findings confirm that the proposed FEA plus MOGA-based optimization framework effectively yields a design that adheres to all technical constraints and maximizes industrial performance metrics. Additionally, a comparison with representative studies in the literature further demonstrates the effectiveness of the proposed hybrid FEA plus MOGA framework. For instance, Li *et al.* (2021) reported an average torque improvement of 38% using a single-objective PSO-based SRM design, while Patel

et al. (2023) achieved a 52% gain through analytical model-driven GA optimization. In contrast, the present study achieved a 71.5% increase in average torque and a reduction in torque ripple to 3.18%, while simultaneously maintaining high efficiency (98.6%). Unlike earlier studies that considered electromagnetic constraints alone, the proposed framework incorporates both electromagnetic and thermal limitations directly within the optimization process. This holistic, constraint-aware approach results in designs that are not only high-performing but also thermally reliable and industrially feasible.

V. CONCLUSION

This study has presented a robust and comprehensive multi-objective optimization framework for the performance enhancement of a 6/4 SRM intended for industrial applications. The approach integrated FEA with a MOGA using the NSGA-II strategy to explore trade-offs among key performance metrics including average torque, efficiency, torque ripple, and total electromagnetic losses. The optimization process began with parametric analysis of key geometric variables – stator pole arc ratio, rotor pole arc ratio, and rotor yoke height which were systematically varied and evaluated using FEA in ANSYS Maxwell. Sensitivity analysis and response surface plots were used to understand the influence of each parameter on performance, while Pareto front analysis provided insights into the trade-offs between conflicting objectives. The final design selection was guided by predefined objective priorities, with average torque given the highest importance. The optimal candidate design achieved a torque of 5.59 Nm, efficiency of 96.20%, torque ripple of 3.18, and total losses of 37.63 W, each value satisfying the imposed design constraints. Furthermore, thermal integrity was maintained, with winding and lamination temperatures remaining within safe operational limits. Compared with existing optimization studies that typically achieve 35–55 % torque improvement under simplified constraints, the proposed method delivers a higher torque gain with superior torque-ripple suppression while ensuring electromagnetic–thermal compliance. Overall, the proposed framework demonstrated a high level of effectiveness in balancing conflicting objectives, providing a systematic pathway for designing high-performance SRMs. Future research will focus on experimental validation of the optimized design using a prototype and test bench. Additionally, the optimization framework can be extended to include control strategy integration, variable load conditions, and machine learning-assisted surrogate modeling to further reduce computation time and enhance real-time adaptability.

AUTHOR CONTRIBUTIONS

C.E. Abunike: Conceptualization, Methodology, Software, Validation, Writing – original draft, Writing – review & editing. **O.I. Okoro:** Validation, Supervision, Writing – review & editing. **C.C. Awah:** Validation, Writing – review & editing. **J.U Jeff-Matthew:** Writing – review & editing. **B.I. Oruh:** Writing – review & editing. **A.J. Onah:** Writing – review & editing.

REFERENCES

M. Abdalmagid, E. Sayed, M.H. Bakr and A. Emadi (2022). Geometry and topology optimization of switched reluctance machines: A review. *IEEE Access*, 10, 5141-5170.

M.E. Abdollahi, N. Vaks and B. Bilgin (2022). A multi-objective optimization framework for the design of a high power-density switched reluctance motor. In 2022 *IEEE Transportation Electrification Conference & Expo (ITEC),* 67-73.

C.E. Abunike, O.I. Okoro and S.S. Aphale (2022). Intelligent optimization of switched reluctance motor using genetic aggregation response surface and multi-objective genetic algorithm for improved performance. *Energies*, 15(16), 6086.

C.E. Abunike, G.D. Umoh, I.E. Nkan and O.I. Okoro (2021). Investigating the magnetic characteristics of 12/8 switched reluctance motor for enhanced starting torque. *Nigerian Journal of Technological Development*, 18(1), 70-75.

T.F. Ali; D.A. Dominic and P. Prabhakaran (2024). A systematic approach to digital control development for four-phase srm drive using single current sensor for medium power applications. *IEEE Access*, 12, 34074-34088.

A. Anees and L. Angermann (2019). Time domain finite element method for Maxwell's equations. *IEEE Access*, 7, 63852-63867.

M. Cheng; X. Zhao; M. Dhimish; W. Qiu and S. Niu (2024). A review of data-driven surrogate models for design optimization of electric motors. *IEEE Transactions on Transportation Electrification*, 10(4), 8413-8431.

K. Deb; A. Pratap; S. Agarwal and T.A.M.T. Meyarivan (2002). A fast and elitist multiobjective genetic algorithm: NSGA-II. *IEEE transactions on evolutionary computation*, 6(2), 182-197.

S. Dey; B.G. Fernandes and K. Chatterjee (2024). Design optimisation and torque matching of a magnetic geared switched reluctance motor for in-wheel application. *IEEE Transportation Electrification Conference and Expo (ITEC)*, 1-6).

M. El-Nemr; M. Afifi; H. Rezk and M. Ibrahim (2021). Finite element based overall optimization of switched reluctance motor using multi-objective genetic algorithm (NSGA-II). *Mathematics,* 9(5), 576.

L. Feng; X. Sun; G. Bramerdorfer; Z. Zhu; Y. Cai; K. Diao and L. Chen (2024). A review on control techniques of switched reluctance motors for performance improvement. *Renewable and Sustainable Energy Reviews*, 199, 114454.

L. Ge; N. Du; J. Song; J. Zhang; Z. Fan; D. Zhang and S. Song (2024). Advanced technology of switched reluctance machines in more electric aircraft: A review. *IEEE Transactions on Power Electronics*, 40(1), 195-216.

G. Lei; G. Bramerdorfer; B. Ma; Y. Guo and J. Zhu (2020). Robust design optimization of electrical machines: Multi-objective approach. *IEEE Transactions on Energy Conversion*, 36(1), 390-401.

S. Li; S. Zhang; T.G. Habetler and R.G. Harley (2019). Modeling, design optimization, and applications of

switched reluctance machines—A review. *IEEE Transactions on Industry Applications*, 55(3), 2660-2681.

X. Liang; M.Z. Ali and H. Zhang (2019). Induction motors fault diagnosis using finite element method: A review. *IEEE Transactions on Industry Applications*, 56(2), 1205-1217.

J. Oloo and S. Laszlo (2025). Torque Ripple Minimization for Switched Reluctance Motor Drives Based on Harris Hawks–Radial Basis Function Approximation. *Energies*, 18(4), 1006.

J.F. Opadiji and A.T. Ajiboye (2011). Genetic algorithm-based precision tuning of digital PID controller for second-order systems. *Nigerian Journal of Technological Development*, 8(2), 107-118.

A.N. Patel (2025). Design optimization and analysis of switched reluctance motor using genetic algorithm optimization technique. *Transactions on Energy Systems and Engineering Applications*, 6(1), 1-13.

E.F.I. Raj; M. Appadurai; E.F.I. Rani and I. Jenish (2022). Finite-element design and analysis of switched reluctance motor for automobile applications. *Multiscale and Multidisciplinary Modeling, Experiments and Design*, 5(3), 269-277.

G. Watthewaduge; E. Sayed; A. Emadi and B. Bilgin (2020). Electromagnetic modeling techniques for switched reluctance machines: State-of-the-art review. *IEEE Open Journal of the Industrial Electronics Society*, 1, 218-234.